

ARRAYS OF VORTICES FOR PARTICLE TRAPPING AND PATTERNING USING SINGLE-BEAM ACOUSTIC HOLOGRAMS

Gabriela Sánchez-Rodríguez¹, Noé Jiménez¹, Sergio Jiménez-Gambín¹, Francisco Camarena¹

¹ Instituto de Instrumentación para Imagen Molecular (I3M), CSIC - Universitat Politècnica de València, Valencia, Spain
email: nojigon@upv.es

Resumen

Las pinzas acústicas suscitan un gran interés en aplicaciones biomédicas, ya que permiten la manipulación de partículas sin contacto para una amplia gama de tamaños utilizando dispositivos de baja potencia, convirtiéndose en herramientas versátiles y poderosas para fines como la manipulación de células o la administración de fármacos. En este trabajo presentamos un novedoso método para generar pinzas acústicas a través de conjuntos de trampas de vórtice acústico para la manipulación de múltiples partículas utilizando lentes holográficas. Asimismo, este enfoque altamente sintonizable permite cambiar la distancia entre las trampas acústicas tan solo variando la frecuencia del haz de ultrasonidos. En primer lugar, presentamos el diseño de la lente holográfica basado en la configuración deseada del conjunto de trampas acústicas en base a la teoría y las simulaciones. Segundo, evaluamos el rendimiento de las trampas excitando el holograma con una onda plana mediante un transductor ultrasónico de elemento simple. Los resultados muestran que los hologramas acústicos permiten la generación de trampas de vórtice acústico con un patrón arbitrario para controlar conjuntos de partículas utilizando un dispositivo de bajo costo y baja potencia. El presente trabajo abre las puertas para aplicaciones en bioingeniería con ultrasonidos para la manipulación de células y control de patrones de portadores de fármacos.

Palabras clave: Vórtices, fuerza de radiación, levitación, elastografía, ultrasonidos.

Abstract

Acoustic tweezers are of great interest to biomedical applications as they allow contactless particle manipulation for a broad range of sizes using low-power devices, becoming versatile and powerful tools for purposes such as cell manipulation or drug delivery. We report a novel method to generate acoustic tweezers through arrays of acoustic-vortex traps using holographic lenses for multiple particle patterning and manipulation. Likewise, this highly tunable approach allows to change the distance between acoustic traps varying the emitter frequency. First, we present the design of the holographic lens based on the desired configuration of acoustic traps based on theory and simulations. Second, we evaluate the trapping performance by exciting the hologram with a plane wave from a single-beam ultrasonic transducer. The results show that acoustic holograms allow generating acoustic-vortex traps with arbitrary lattice-pattern to control arrays of particles using a low-cost and low-power device. We advance applications in ultrasound bioengineering for cell-manipulation or drug-delivery carrier patterning.

Keywords: Vortex, acoustic radiation force, levitation, elastography, ultrasound.

PACS nº. 43.80.Sh, 43.60.Sx

1 Introduction

Acoustic streaming (i.e. acoustic vortex generation) has been substantially studied in the past years, as acoustic waves can interact with objects non-destructively, being able to penetrate deeper than light waves [1]. This form of acoustical tweezing shows great potential as it allows to manipulate large particles through low power devices [2]. Additionally, it has been shown that acoustic vortices transfer orbital momentum to matter in the free field which results in torque-induction for solids and azimuthal rotation induction for fluids thus enabling a wide range of applications, including therapeutic applications, which require from these non-invasive mechanical effects [3]. However, current technologies based on helical sources [4], spiral gratings [5-6] or metasurfaces [7] are not able to reproduce simultaneously multiple vortex traps, and phased array systems [8] can only reproduce a small number of vortices due to the limited number of active elements.

Hereby, we present a novel method for the generation of acoustic vortex traps through holographic lenses which have been shown to generate complex acoustic fields even in inhomogeneous media, providing precise control and making this approach suitable for medical applications [9]–[11]. We demonstrate the capability of producing desired vortex target field, with a semi-analytical method using the Rayleigh-Sommerfeld diffraction integral, to firstly creating the vortex holographic lens through back-propagation and then using forward-propagation to show how this lens effectively generates the target field. This work blazes the trail for biomedical applications of ultrasound in the field of particle manipulation, with high potential for the design of drug delivery systems within the human body.

2 Methods

The process of hologram generation is comprised of four steps. First, we design the target field as shown in Fig.1 (a), where we indicate the number and position of each vortex. Second, we perform back-propagation from the target towards the source capturing the holographic information by using the Rayleigh-Sommerfeld propagation integral as shown in Fig. 1 (b) through the Rayleigh-Sommerfeld propagation integral. Third, we design the holographic lens using the phase-conjugated field as shown in Fig. 1 (c). Finally, we excite the hologram with a plane wave to evaluate the result as shown in Fig. 1 (d). In the following lines we give a brief description of the procedure followed, however, the reader is referred to Refs [9]–[11] for a more detailed description of the process.

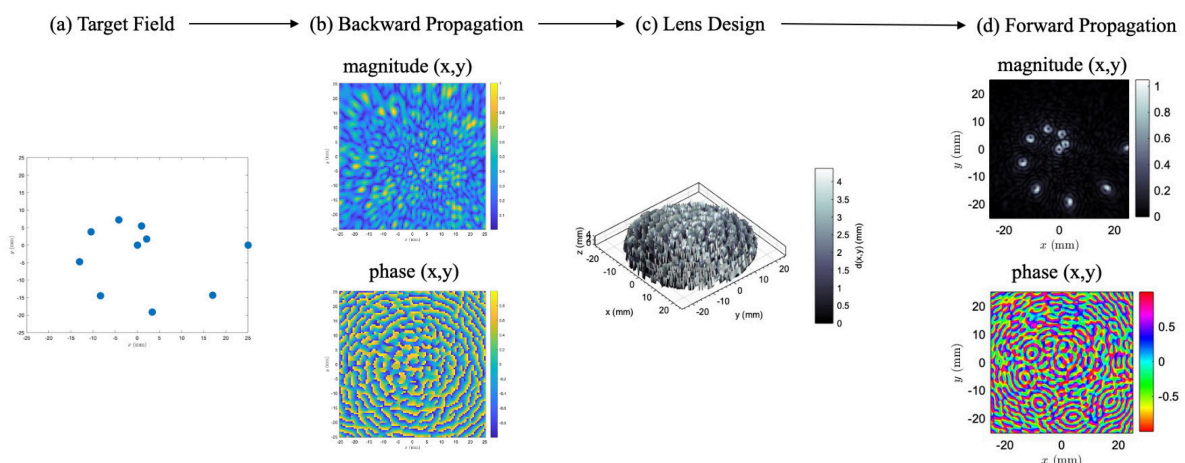


Figure 1. Hologram generation process. (a) Selected target field. (b) Back-propagation of the target field. (c) Designed lens. (d). Forward propagation from the lens.

2.1 Backward propagation

To design the holographic lens, we estimate the backward-propagated acoustic field using a semi-analytical method based on the Rayleigh-Sommerfeld diffraction integral. These theoretical calculations are performed in homogeneous media, i.e., in water. The acoustic pressure field $p(\mathbf{r})$ at a point \mathbf{r} generated by a moving surface S of arbitrary shape located at coordinates \mathbf{r}_0 and vibrating with a complex particle velocity $v_0(\mathbf{r}_0)$ normal to the surface is given by the Rayleigh-Sommerfeld integral as

$$p(\mathbf{r}, \omega) = \frac{i\omega\rho_0}{2\pi} \int_S \frac{v_0(\mathbf{r}_0) \exp(-k_0 |\mathbf{r} - \mathbf{r}_0|)}{|\mathbf{r} - \mathbf{r}_0|} dS, \quad (1)$$

where $\omega = 2\pi f$, $k_0 = \omega/c_0$ and ρ_0 are the angular frequency, wavenumber and density, respectively, of a homogeneous media with sound speed given by c_0 [12].

To synthesize the lattice of vortices, we first define a lattice of target locations whose coordinates are given by x_n and y_n . To generate each vortex of topological charge l at each target location, we introduce a set of 30 virtual sources distributed along a ring of radius $r_v = (l + 0.8086 \sqrt[3]{l})/k_r$ surrounding each target location, where the transverse wavenumber is given by $k_r = k_0 a / (F \sqrt{[a^2/F^2] + 1})$, F is the focal plane of the lens and a is the aperture. Therefore, each virtual source is located at $x_v = r_v \cos(\theta_v)$ and $y_v = r_v \sin(\theta_v)$, where $\theta_v = \tan^{-1}(y_v - y_n)/(x_v - x_n)$ is the polar angle with respect to the target location. Finally, we set a complex amplitude of $\exp(il\theta_v)$ for each virtual source. Therefore, an arbitrary set of vortices centered at arbitrary positions, as the example shown in Fig. 1(a), can be backpropagated by using Eq. (1) to the location of the holographic surface to obtain the amplitude and phase patterns shown in Fig. 1 (b). This holographic information is used to manufacture the physical lens.

2.2 Lens design

The lens plane matches the location of the holographic plane and should encode the patterns retrieved by the backpropagation method. In this work we use a phase-only lens to encode the complex-conjugated backpropagated field, under the assumption of reciprocity, time-invariance, and linearity of the system. To design the physical holographic lens, we divide the lens in squared pixels of height $h(x_0, y_0)$. We assume each column vibrates longitudinally as an elastic Fabry-Pérot resonator. Therefore, locally transmitted waves at the output plane of the lens, z_0 , present a complex and frequency dependent transmission coefficient given by [3]

$$T(x_0, y_0) = \frac{2Z_n \exp(-ik[z_0 - h])}{2Z_n \cos(k_L h) + i(2Z_n^2 + 1) \sin(k_L h)} \quad (2)$$

where $k_L = \omega/c_L$ is the wavenumber in the lens, $Z_n = Z_L/Z_0$ is the normalized lens impedance, $Z_0 = \rho_0 c_0$ and ρ_0 the impedance and density of water, respectively, and $Z_L = \rho_L c_L$, c_L and ρ_L are the impedance, speed of sound and density of the lens, respectively. We use Eq. (2) to obtain the set of pixel height, $h(x_0, y_0)$, that produce a matching between the phase of the transmitted waves and the phase of the complex-conjugated backpropagated field, i.e., $\arg[T(x_0, y_0)] = \arg[p^*(x_0, y_0)]$. Because Eq. (2) is non-invertible due to trigonometric reasons, we perform a numerical evaluation of the expression in a test curve, that is, for a broad range of pixel heights, starting from a minimum until a given height that provides a phase of the transmission coefficient is greater than 2π . Then, we perform a linear interpolation to obtain the height of the pixel as a function of the required phase.

As an example, to obtain the physical holographic lens sketched in Fig. 1(c), a set of virtual sources were spatially distributed with a separation $\lambda/3$ all over the target field, Fig. 1 (a), and we recorded the patterns shown in Fig. 1 (b) at the holographic surface. Then, the surface is divided in squared pixels

and using the complex-conjugated backpropagated field calculated by Eq. (1) the height of each of columns is calculated using Eq. (2). For more detailed information, we refer the reader to Refs. [9-11].

The parameters introduced for the lens were based on SOMOS watershed XC11122, a resin used for stereolithography. The introduced parameters were the Young modulus (2.88 GPa), Poisson's ratio (0.4) and density ($\rho_L = 1200 \text{ kg/m}^3$) of the material, leading to a sound speed of $c_L = 2270 \text{ m/s}$, 1.5 times higher than in water, and an impedance of $Z_L = 2.72 \text{ MRayls}$, 1.8 times higher than in water. We use a lens with an aperture of $2a = 50 \text{ mm}$ and a central frequency of $f = 1 \text{ MHz}$ in water.

2.3 Forward propagation

Once the lens was created, forward propagation was computed to assess the performance of the lens and check that we obtained a replica of the target field. To perform this, we integrated equation Eq. (1) forwards. Besides the magnitude and phase in the x - y plane, we computed a sagittal cross-section in the x - z plane to evaluate the focusing performance of the lens out of the focal plane.

3 Results

We show the theoretical results obtained for three different target fields: a set of vortices located at random positions, a lattice of vortices following an Archimedean spiral lattice and a Vogel's spiral pattern to reproduce a tightly-packed vortex distribution.

3.1 Arbitrary set of vortices

First, we set a random pattern of few vortices ($N = 3$). The targets are shown in Fig. 2 (a). After applying the process described in methods a lens is obtained [Fig.2 (f)]. Using this lens we retrieve the acoustic field at the focal plane, shown in Figs. 2(b,c). One vortex is focused at each target with high fidelity. A ring-shaped structure is shown in the magnitude of the field while at each location the phase rotates a total of $2\pi l$ times along the center of each vortex, with $l = 1$, therefore focused vortices with the design topological charge are correctly synthesized. One can note that the vortices located far away from the center e.g., $y = 20 \text{ mm}$, are also synthesized, but as they are near the source boundary (the radius of the source is 25 mm), they present a magnitude distribution that differs from a uniform ring. However, the phase is correctly reproduced, and a singularity is observed at the center. The sagittal cross-section is given in Fig. 2(d), where a sharp focusing is observed for the central vortex.

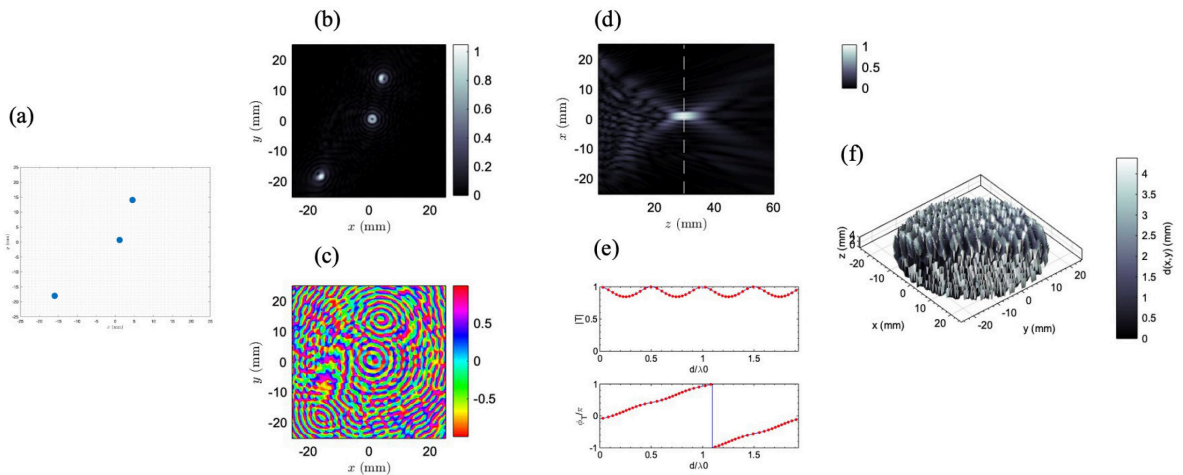


Figure 2: Arbitrary pattern of vortices. (a) Desired coordinates of vortices (target field). (b,c) Magnitude and phase, respectively, of the resulting forward-propagated field using the holographic lens. (d) Axial plane in the forward-propagated field at $y=0 \text{ mm}$. (e) Above: magnitude of the transmitted waves for a test curve using Eq.(2) (continuous-blue line) and transmission at different pixels (dotted-red line). Below: corresponding phase. (f) Designed lens.

3.2 Archimedean spiral lattice

We can set different target distributions as the Archimedean spiral lattice. The coordinates for the n -th point of the sequence are given by

$$\begin{aligned} r_n &= \alpha \theta_n^\gamma, \\ \theta_n &= 2\pi\beta n, \end{aligned} \quad (3)$$

where α , β and γ are constants, and $n = 1, 2, 3, \dots$. Results are shown in Fig. 3, where a good agreement is observed between the target and resulting field. In addition, one might note that the sagittal field distribution, given in Fig. 3(d), presents a sharp focusing at the plane $z = F$ because of the coarse lattice used. However, the tightly packed vortices at the center ($x = 0$ and $y = 0$) results in an unresolved interference pattern and vortices at this location are not sharply focused.

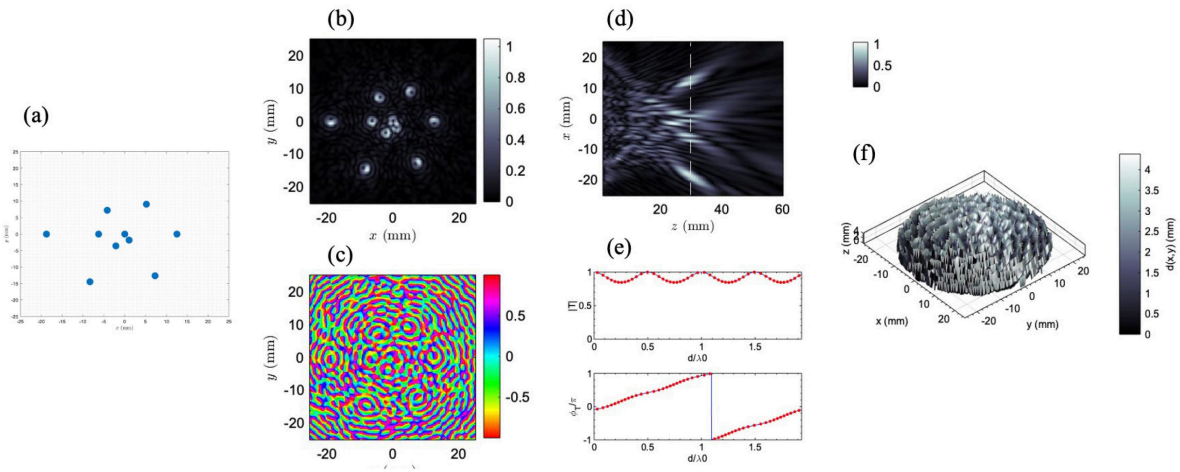


Figure 3: Archimedean spiral pattern of vortices. (a) Desired coordinates of vortices (target field). (b,c) Magnitude and phase, respectively, of the resulting forward-propagated field using the holographic lens. (d) Axial plane in the forward-propagated field at $y=0$ mm. (e) Above: magnitude of the transmitted waves for a test curve using Eq. (2) (continuous-blue line) and transmission at different pixels (dotted-red line). Below: corresponding phase. (f) Designed lens.

3.3 Vogel's spiral lattice

To go further and produce a tightly-packed cluster of vortices, we use a lattice given by the Vogel's spiral. This lattice presents several remarkable features, on the one hand it provides a very efficient packing while, on the other hand, the distribution of points is aperiodic. The distribution of points, in polar coordinates, is given by for the n -th point of a sequence is given by

$$\begin{aligned} r_n &= \beta\sqrt{n}, \\ \theta_n &= \theta_\varphi n, \end{aligned} \quad (4)$$

where $\theta_\varphi = 2\pi/\varphi^2$ is the golden angle, $\varphi = (1 + \sqrt{5})/2$ is the golden ratio, β is a constant and $n = 1, 2, 3, \dots$. The coordinates of each vortex are then given by $x_n = r_n \cos(\theta_n)$ and $y_n = r_n \sin(\theta_n)$.

Fig. 4 shows the field generated by a lens designed to generate a Vogel's lattice. The results show a very good agreement between the reconstructed field and the target location. In addition, at the center of each target we can identify in the field magnitude [see Fig.4(b)] a ring-shaped structure whose phase [see

Fig.4(c)] rotates along the center a number of times that corresponds to the design topological charge, i.e., $l = 1$. The sagittal cross-section is given in Fig. 4(d) where it can be observed that the energy is also focused out of the focal plane. In fact, designing a hologram using a direct method to generate an image at a given plane does not guarantee that the energy focuses in other focal planes.

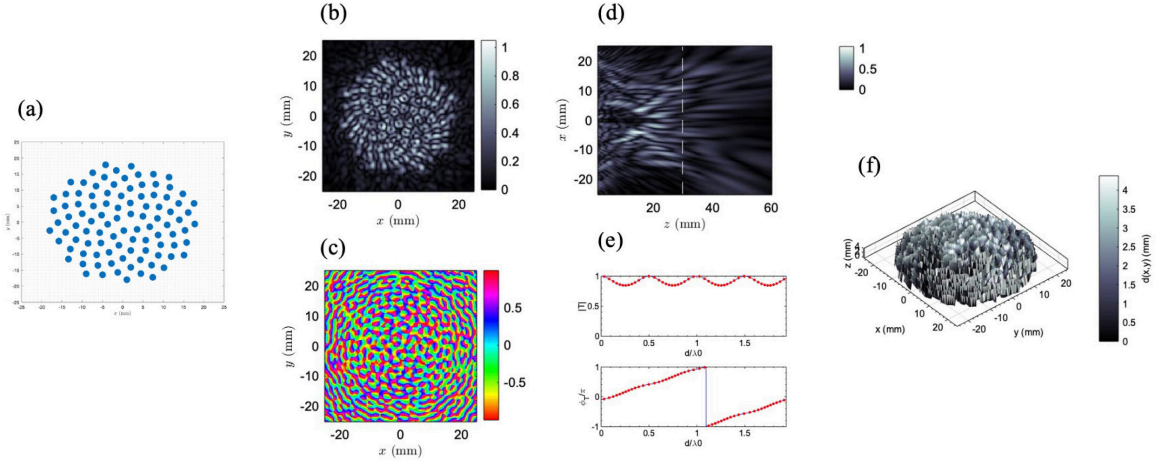


Figure 4: Vogel's pattern of vortices. (a) Desired coordinates of vortices (target field). (b,c) Magnitude and phase, respectively, of the resulting forward-propagated field using the holographic lens. (d) Axial plane in the forward-propagated field at $y=0$ mm. (e) Above: magnitude of the transmitted waves for a test curve using Eq. (2) (continuous-blue line) and transmission at different pixels (dotted-red line). Below: corresponding phase. (f) Designed lens.

4 Conclusions

We have shown that multiple acoustic-vortex traps located at arbitrary positions can be generated using holographic lenses. We encode very complex holographic acoustic fields into a single lens, and by using a single-element transducer the resulting field matches the target distribution of vortex traps with great accuracy. The presented approach is highly tunable and can be applied to arbitrary lattices of arbitrary topological charges. This proposal outperforms current approaches based on phased arrays or spiral gratings for multiple vortex trapping and, in addition, it results in a simple, robust and low-cost system. This work will pave the road for the application of ultrasonic vortex-trapping technologies in drug delivery, cell and particle manipulation systems in biomedical applications, or in underwater communications based on vortex encoding.

Acknowledgements

This research has been supported by the Spanish Ministry of Science, Innovation and Universities through grant "Juan de la Cierva - Incorporación" (IJC2018-037897-I) and PID2019-111436RB-C22, by the Agència Valenciana de la Innovació through grant INNVA1/2020/92 and INNCON/2020/009. Action co-financed by the European Union through the Programa Operativo del Fondo Europeo de Desarrollo Regional (FEDER) of the Comunitat Valenciana 2014-2020 (IDIFEDER/2018/022).

References

- [1] Y. Li, G. Guo, Q. Ma, J. Tu, and D. Zhang, “Deep-level stereoscopic multiple traps of acoustic vortices,” *J. Appl. Phys.*, 2017, doi: 10.1063/1.4981122.
- [2] J.-L. T. R. M. D Baresch, “Observation of a single-beam gradient force acoustical trap for elastic particles: acoustical tweezers,” *Phys. Rev. Lett.*, vol. 116, p. 024301, 2016.
- [3] A. Riaud, M. Baudoin, J. L. Thomas, and O. Bou Matar, “Cyclones and attractive streaming generated by acoustical vortices,” *Phys. Rev. E - Stat. Nonlinear, Soft Matter Phys.*, vol. 90, no. 1, p. 13008, 2014, doi: 10.1103/PhysRevE.90.013008.
- [4] B. T. Hefner and P. L. Marston, “An acoustical helicoidal wave transducer with applications for the alignment of ultrasonic and underwater systems,” *J. Acoust. Soc. Am.*, vol. 106, no. 6, pp. 3313–3316, 1999, doi: 10.1121/1.428184.
- [5] N. Jiménez, V. Romero-García, L. M. García-Raffi, F. Camarena, and K. Staliunas, “Sharp acoustic vortex focusing by Fresnel-spiral zone plates,” *Appl. Phys. Lett.*, vol. 112, no. 20, p. 204101, May 2018, doi: 10.1063/1.5029424.
- [6] N. Jiménez, R. Picó, V. Sánchez-Morcillo, V. Romero-García, L. M. García-Raffi, and K. Staliunas, “Formation of high-order acoustic Bessel beams by spiral diffraction gratings,” *Phys. Rev. E*, vol. 94, no. 5, p. 053004, Nov. 2016, doi: 10.1103/PhysRevE.94.053004.
- [7] X. Jiang, Y. Li, B. Liang, J. C. Cheng, and L. Zhang, “Convert Acoustic Resonances to Orbital Angular Momentum,” *Phys. Rev. Lett.*, vol. 117, no. 3, p. 34301, 2016, doi: 10.1103/PhysRevLett.117.034301.
- [8] A. Marzo, S. A. Seah, B. W. Drinkwater, D. R. Sahoo, B. Long, and S. Subramanian, “Holographic acoustic elements for manipulation of levitated objects,” *Nat. Commun.*, vol. 6, p. 8661, 2015.
- [9] S. Jiménez-Gambín, N. Jiménez, J. M. Benlloch, and F. Camarena, “Holograms to Focus Arbitrary Ultrasonic Fields through the Skull,” *Phys. Rev. Appl.*, vol. 12, no. 1, p. 014016, Jul. 2019, doi: 10.1103/PhysRevApplied.12.014016.
- [10] S. Jiménez-Gambín, N. Jiménez, J. M. Benlloch, and F. Camarena, “Generating Bessel beams with broad depth-of-field by using phase-only acoustic holograms,” *Sci. Rep.*, vol. 9, no. 1, p. 20104, Dec. 2019, doi: 10.1038/s41598-019-56369-z.
- [11] S. Jiménez-Gambín, N. Jiménez, J. M. Benlloch, and F. Camarena, “Transcranial focusing of ultrasonic vortices by acoustic holograms,” *Preprint*, 2020.
- [12] D. T. Blackstock, *Fundamentals of physical acoustics*. John Wiley & Sons, 2000.